Electronic Supplementary Material (ESI) for Journal of Materials Chemistry A.
This journal is © The Royal Society of Chemistry 2022

Supporting Information

Highly Efficient Ternary Solar Cells with Reduced Non-radiative Energy Loss and Enhanced Stability via Two Compatible Non-fullerene Acceptors

Xin Yan,[a] Jingnan Wu,[a,b] Junfang Lv,[a] Liu Zhang,[a] Rui Zhang,[c] Xia Guo,[a] Maojie Zhang*[a]

[a]Laboratory of Advanced Optoelectronic Materials, Suzhou Key Laboratory of Novel Semiconductor-optoelectronics Materials and Devices, College of Chemistry, Chemical Engineering and Materials Science, Soochow University, Suzhou 215123, China

E-mail: mjzhang@sdu.edu.cn

[b]Department of Chemistry and Bioscience, Aalborg University, DK-9220 Aalborg, Denmark

[c]Department of Physics, Chemistry and Biology (IFM), Linköping University, Linköping, Sweden

Materials and Methods

Materials

All chemicals and solvents were reagent grades and purchased from Damas-beta, Acros Organics, and Sigma-Aldrich. PM6 and MOIT-M were synthesized according to the previous literature.[1,2] BTP-eC9 was purchased from Solarmer Materials Inc.

DSC, UV-Vis-NIR absorption, CV, and PL measurements

Differential scanning calorimetry (DSC) was performed on a TA DSC Q-200. Ultraviolet-visible-near infrared (UV-Vis-NIR) absorption spectra was taken on an Agilent Technologies Cary 5000 Series UV-Vis-NIR Spectrophotometer. Cyclic voltammetry (CV) was performed on a Zahner Zennium IM6 electrochemical workstation with a three-electrode system in 0.1 mol/L Bu_4NPF_6 acetonitrile solutions at a scan rate of 50 mV/s. The three-electrode system included a glassy carbon disk, platinum wire, and Ag/Ag^+ electrode as the working electrode, counter electrode, and reference electrode, respectively. The potential of the Ag/Ag^+ reference

electrode was internally calibrated by using the ferrocene/ferrocenium redox couple (Fc/Fc^+), and the Ag/Ag^+ reference electrode possessed an energy level of 4.73 eV. Photoluminescence (PL) spectra was performed on an Edinburgh Instrument FLS 980.

***J-V* and EQE measurements**

The current density-voltage (*J-V*) characteristics were recorded with a Keithley 2450. The power conversion efficiencies were measured under 1 sun, AM 1.5G (air mass 1.5global) (100 mW/cm^2) using an SS-F5-3A (Enli Technology CO., Ltd.) solar simulator (AAA grade, 50 mm×50 mm photo-beam size). 2×2 cm^2 Monocrystalline silicon reference cell (SRC-00019, covered with a KG5 filter window) was purchased from Enli Technology CO., Ltd. The EQE was measured by Solar Cell Spectral Response Measurement System QE-R3011 (Enli Technology CO., Ltd.). The light intensity at each wavelength was calibrated with a standard single-crystal Si photovoltaic cell.

SCLC mobility measurement

The hole and electron mobilities of devices were evaluated from the space-charge-limited current (SCLC) method with the hole-only structure of ITO/PEDOT:PSS/blend films/MoO_3/Ag and electron-only structure of ITO/ZnO/blend films/PFN-Br/Ag, respectively. The corresponding charge mobilities were calculated from fitting the Mott-Gurney square law $J = 9\varepsilon_r\varepsilon_0\mu V^2/(8L^3)$, where J is the current density, ε_r is the dielectric permittivity of the active layer (assumed to be 3), ε_0 is the vacuum permittivity, L is the thickness of the active layer, μ is the hole or electron mobility. $V = V_{appl} - V_{bi} - V_s$, V_{appl} is the applied voltage, V_{bi} is the built-in voltage, V_s is the voltage drop from the substrate's series resistance ($V_s = IR$). The SCLC devices were measured under a dark condition in a nitrogen glovebox without encapsulation.

Energy loss measurement

FTPS-EQE was measured by using an integrated system (PECT-600, Enlitech), where the photocurrent was amplified and modulated by a lock-in instrument. EQE_{EL} measurement was

performed by applying external voltage/current sources through the devices (ELCT-3010, Enlitech).

$$E_{\text{loss}} = E_{\text{g}}^{\text{PV}} - qV_{\text{oc}}$$

$$= \left(E_{\text{g}}^{\text{PV}} - qV_{\text{oc}}^{\text{SQ}}\right) + \left(qV_{\text{oc}}^{\text{SQ}} - qV_{\text{oc}}^{\text{rad}}\right) + \left(qV_{\text{oc}}^{\text{rad}} - qV_{\text{oc}}\right)$$

$$= \left(E_{\text{g}}^{\text{PV}} - qV_{\text{oc}}^{\text{SQ}}\right) + q\Delta V_{\text{oc}}^{\text{rad, below gap}} + q\Delta V_{\text{oc}}^{\text{non - rad}}$$

$$= \Delta E_1 + \Delta E_2 + \Delta E_3$$

Where VSQ ocis the maximum voltage according to the Shockley-Queisser limit, Vrad ocis the open-circuit voltage when there is only radiative recombination.

$$qV_{\text{oc}}^{\text{SQ}} = \text{kTln}\left(\frac{J_{\text{sc,SQ}}}{J_{0,\text{SQ}}} + 1\right) = \text{kTln}\left(\frac{\text{e}\int_{\text{E}_\text{g}}^{\infty} \text{Ø}_{\text{AM1.5}}(E)\text{d}E}{\text{e}\int_{\text{E}_\text{g}}^{\infty} \text{Ø}_{\text{bb}}(E)\text{d}E} + 1\right)$$

where $\varnothing_{\text{AM1.5}}$ is the solar radiation photon flux, $\varnothing_{\text{bb}}$ is the black body radiation at 300K.

$$qV_{\text{oc}}^{\text{rad}} = \text{kTln}\left(\frac{J_{\text{sc}}}{J_{0,\text{rad}}} + 1\right) = \text{kTln}\left(\frac{q\int_{0}^{\infty} \text{EQE}\text{Ø}_{\text{AM1.5}}(E)\text{d}E}{q\int_{0}^{\infty} \text{EQE}\text{Ø}_{\text{bb}}(E)\text{d}E} + 1\right)$$

$$q\Delta V_{\text{oc}}^{\text{non - rad}} = -\text{kTln}(\text{EQE}_{\text{EL}})$$

EQE_{EL} is the electroluminescence quantum efficiency.

AFM and TEM measurements

Atomic force microscopy (AFM) measurement was obtained by using Dimension 3100 (Veeco) Atomic Force Microscope in a tapping mode. Transmission electron microscopy (TEM) was performed on a Tecnai G2 F20 S-TWIN instrument at 200 kV accelerating voltage, in which the blend films were prepared as follows: first, the blend films were spin-coated on the PEDOT:PSS/ITO substrates; second, the resulting blend film/PEDOT:PSS/ITO substrates

were submerged in deionized water to make these blend films float onto the air-water interface; finally, the floated blend films were taken up on unsupported 200 mesh copper grids for a TEM measurement.

TPC and TPV measurements

Transient photovoltage (TPV) and transient photocurrent (TPC) measurements were carried out under a 337 nm 3.5 ns pulse laser (160 μJ per pulse at 10 Hz) and halide lamps (150 W). Voltage and current dynamics were recorded on a digital oscilloscope (Tektronix MDO3102).

GIWAXS measurement

Grazing incident wide-angle X-ray scattering (GIWAXS) data was obtained from NCD-SWEET beamline, ALBA Synchrotron, Spain. The energy of the X-ray beam was set to 12.95 keV using a Si (111) channel-cut monochromator and further collimated with an array of Be lenses. The incidence angle was 0.14° and the diffraction patterns were collected using a Rayonix LX255-HS area detector, which consists of a pixel array of 5760×1920 (V×H) with a pixel size of 88.54×88.54 μm^2 for the pixel binning employed of 2×2. The scattering vector q was calibrated using Cr_2O_3 as standard, obtained using a sample to detector distance of 0.23 m.

Contact angle measurement

The contact angle test was performed on a Dataphysics OCA20 Micro surface contact angle analyzer. The surface energy of the polymers was characterized and calculated by the contact angles of the two probe liquids (ultrapure water and diiodomethane) with the Owens and Wendt equation: $\gamma_{LV}(1 + \cos\theta) = 2(\gamma_S^d\gamma_L^d)^{1/2} + 2(\gamma_S^p\gamma_L^p)^{1/2}$, where γ_S and $\gamma_L$are the surface energy of the sample and the probe liquid, respectively. The superscripts d and p refer to the dispersion and polar components of the surface energy, respectively.

To calculate the wetting coefficient (ω), we should know the interfacial surface energy between different components first, which can be calculated by Neumann's equation as follows:

$$\omega_C = \frac{\gamma_{C-B} - \gamma_{C-A}}{\gamma_{A-B}}$$

where $\gamma_{X-Y}$is the interfacial surface energy between X and Y.

The interfacial surface energy can be calculated by Neumann's equation as follows:

$$\gamma_{x-y} = \gamma_x + \gamma_y - 2\sqrt{\gamma_x \cdot \gamma_y} \cdot e^{-\beta(\gamma_x - \gamma_y)^2}$$

where $\beta = 0.000115\ m^4/mJ^2$.

The location of the material C is estimated through ω_C. If $\omega_c < -1$, material C will locate in domain B. If $-1 < \omega_c < -1$, material C will locate at the interface between material A and B. If $\omega_c > 1$, material C will locate in domain A.

Fabrication and Characterization of Polymer Solar Cells.

All the devices with a conventional device structure of ITO/PEDOT:PSS (30 nm)/active layers/PFN-Br (5 nm)/Ag (100 nm) were fabricated under conditions as follows.

The patterned indium tin oxide (ITO) coated glasses were cleaned with detergent and then underwent a wet-cleaning process inside an ultrasonic bath procedure, followed by ultrapure water, acetone, and isopropanol in sequence, and then blown dry through high-purity nitrogen. After the treatment in a UV-Ozone Cleaner for 20 min, PEDOT:PSS (Heraeus Clevios PVP Al 4083) was deposited by spin-coating under 6000 rpm for 40 s on the cleaned ITO substrate. Then the films were annealed at a hot plate of 150 ^oC for 15 min in the air and the substrates were transferred into a glove box immediately. The optimal PM6:BTP-eC9 (1:1.2, w/w), PM6:MOIT-M (1:1.2, w/w) binary blends, and PM6:Y6:MOITIC (1:1.2:0.3, w/w) ternary blends are dissolved in chloroform (CF), which is placed to a hot plate at 50 ^oC stirred for 4 h. We keep the concentration of donor PM6 at 8 mg/ml unchanged. 0.75 vol% of 1,8-diiodooctane (DIO) was added as additive. The blend solution was spin-cast at 4000 ~ 5000 rpm for 50 s over the ITO glasses from a ~ 100 nm thickness of the active layer, followed by 100 ^oC thermal treatment for 10 minutes. Then, the solution of PFN-Br which dissolved in methanol with a

concentration of 0.5 mg/ml was spin-coated over the active layers at 3000 rpm for 30 s. Finally, 100 nm Ag was successively deposited on the active layers under vacuum at a pressure of ca. 3.5×10^{-4} Pa through a shadow mask to determine the active area of the devices (~ 0.04 cm^2).

Supplementary figures and tables

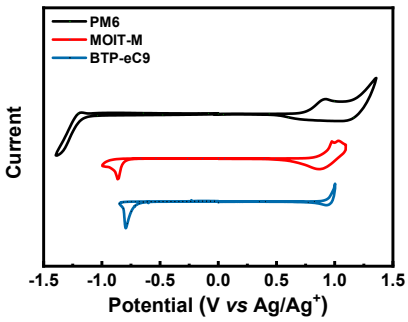

Fig. S1 Cyclic voltammogram of PM6, BTP-eC9 and MOIT-M.

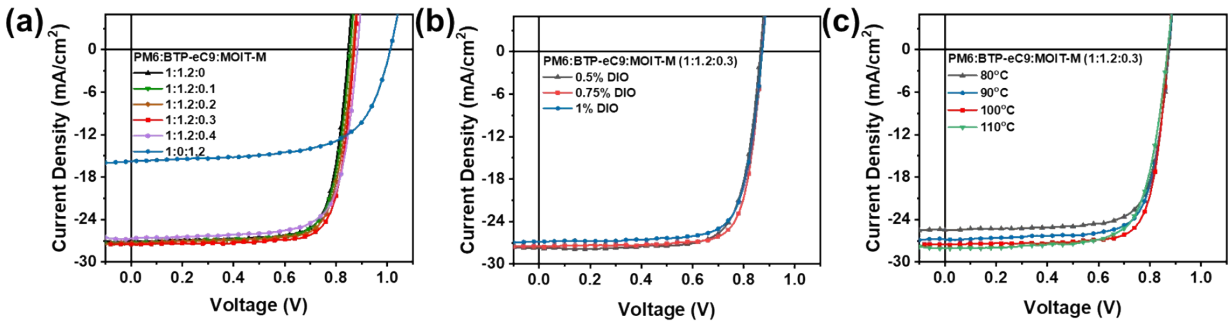

Fig. S2 (a) *J-V* curves of binary and ternary devices with different MOIT-M content. (b) *J-V* curves of ternary devices (1:1.2:0.3, w/w) with different additive contents, and (c) *J-V* curves of ternary devices (1:1.2:0.3, w/w) with different annealing temperatures.

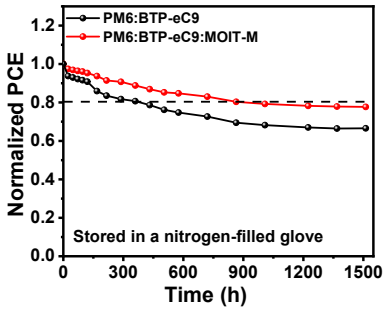

Fig. S3 Storage stability in a nitrogen-filled glove of the un-encapsulated PM6:BTP-eC9 and PM6:BTP-eC9:MOIT-M devices.

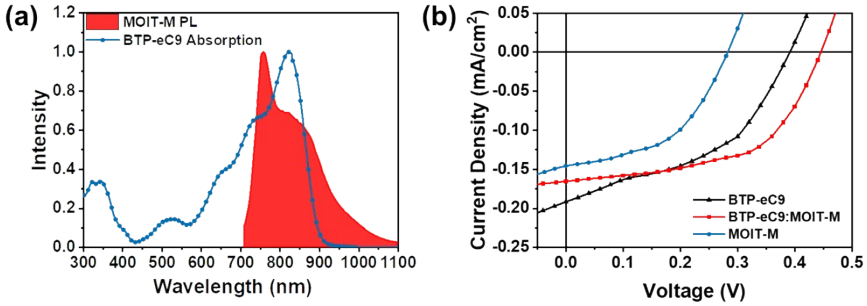

Fig. S4 (a) PL spectra of MOIT-M and UV-vis-NIR absorption spectra of BTP-eC9. (b) *J*-*V* characteristics of OSCs based on BTP-eC9, MOIT-M and BTP-eC9:MOIT-M (1.2:0.3, w/w) films.

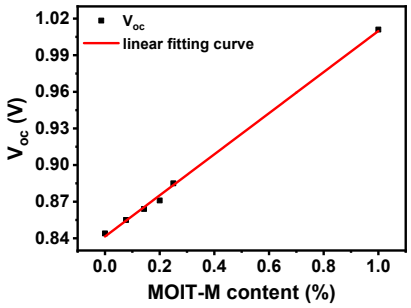

Fig. S5 V_{oc} variation curves of the ternary devices with different MOIT-M contents.

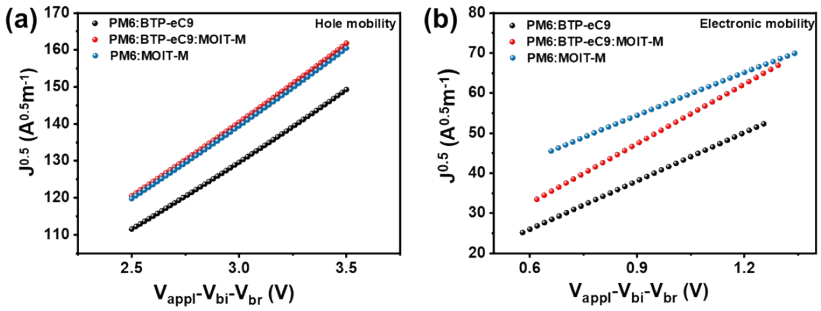

Fig. S6 $J^{1/2}$-V characteristics of (a) hole-only and (b) electron-only devices.

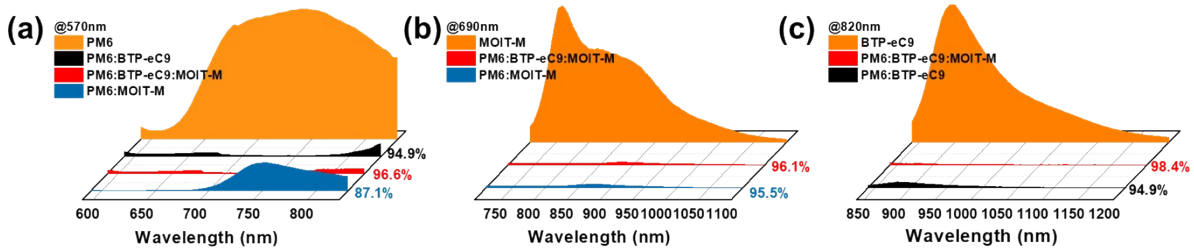

Fig. S7 PL intensities of the pure films and related blend films, excited at (a) 570 nm, (b) 690 nm, and (c) 820 nm.

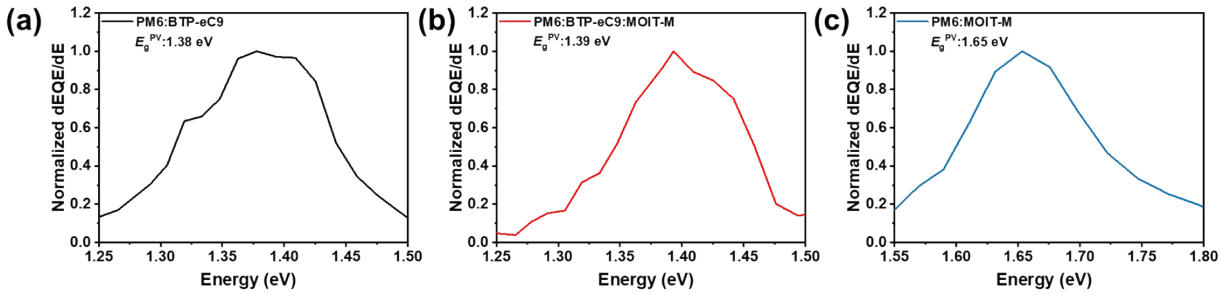

Fig. S8 (a-c) Determination of the *E*PV g of the binary and ternary devices via the derivatives of the EQE spectra.

Table S1. Photovoltaic parameters of the OSCs with different MOIT-M contents (thermal annealing at 100 ℃ for 10 min) under the illumination of AM 1.5G, 100 mW/cm^2.

PM6:BTP-eC9:MOIT-M(w/w)	V_{oc} (V)	J_{sc} (mA/cm^2)	FF (%)	PCE (%)
1:1.2:0	0.84	27.0	76.1	17.4
1:1.2:0.1	0.85	27.2	76.1	17.7
1:1.2:0.2	0.86	27.3	76.4	18.0
1:1.2:0.3	0.87	27.4	77.3	18.5
1:1.2:0.4	0.88	26.6	73.7	17.3
1:0:1.2	1.01	15.8	64.6	10.3

Table S2. Photovoltaic parameters of the ternary OSCs (1:1.2:0.3, w/w) with different DIO contents (thermal annealing at 100 ℃ for 10 min) under the illumination of AM 1.5G, 100 mW/cm^2.

DIO content (%)	V_{oc} (V)	J_{sc} (mA/cm^2)	FF (%)	PCE (%)
0.5	0.86	27.7	75.4	18.0
0.75	0.87	27.4	77.3	18.5
1	0.87	27.0	75.7	17.6

Table S3. Photovoltaic parameters of the ternary OSCs (1:1.2:0.3, w/w) with different annealing temperatures for 10 min under the illumination of AM 1.5G, 100 mW/cm^2.

Temperature (^{o}C)	V_{oc} (V)	J_{sc} (mA/cm^2)	FF (%)	PCE (%)
80	0.87	25.5	75.0	16.7
90	0.87	26.8	75.0	17.6
100	0.87	27.4	77.3	18.5
120	0.87	27.9	72.6	17.6

Table S4. Summary of photovoltaic parameters of the recently reported ternary OSCs.

Host blend	Third component	V_{oc} (V)	J_{sc} (mA/cm^2)	FF (%)	PCE (%)	Ref.
PM6:Y6	BTBR-2F	0.859	27.30	74.1	17.3	[3]
PM6:Y6	S3	0.856	25.86	79.1	17.53	[4]
PM6:Y6	BTTzR	0.870	26.20	77.7	17.70	[5]
D18:Y6	BTPR	0.863	27.65	74.6	17.80	[6]
PM6:Y6	AQx-1	0.853	26.45	77.9	17.86	[7]
PM6:Y6	AQx-3	0.870	26.82	77.2	18.01	[8]
PM6:BTP-eC9	BPR-SCl	0.856	27.13	77.6	18.02	[9]
PM6:BTP-eC9	BTP-F	0.858	26.99	79.7	18.45	[10]
PM6:BO-4Cl	Y6-1O	0.855	27.46	79.0	18.52	[11]
D18-Cl:Y6	G19	0.871	27.36	77.7	18.53	[12]
PM6:BTP-eC9	L8-BO-F	0.853	27.35	80.0	18.60	[13]
PM6:BTP-eC9	BTP-S2	0.878	26.78	79.4	18.66	[14]
PM6:BTP-eC9	AITC	0.870	27.20	79.7	18.80	[15]
PTQ10:m-BTP-PhC6	$PC_{71}BM$	0.869	26.99	80.6	18.89	[16]
PBQx-TF:eC9-2Cl	F-BTA3	0.879	26.70	80.9	19.00	[17]
PM6:BTP-eC9	MOIT-M	0.87	27.4	77.3	18.5	This work

Table S5. Recent progress in the storage stability in a nitrogen-filled condition of ternary OSCs.

Host blend	Third component	PCE_{best} (%)[a]	Storage stability		Ref.
			Time (h)	PCE/PCE_0 (%)[b]	
PM6:BTP-4Cl	PDI-2T[c]	16.32	300	70.10	[18]
PM6:BTP-4Cl	DRCN5T[c]	16.83	300	78.13	[18]
PM6:Y6	$PC_{71}BM$[d]	16.67	200	80	[19]
PM6:Y6	TF1[d]	16.91	648	70	[20]
PM6:Y6	PTO2[e]	17.05	1700	90	[21]
PM6:BTP-4F-12	MeIC[c]	17.4	500	91	[22]
PM6:Y6	BTTzR[d]	17.7	720	93	[5]
PM6:Y6	AQx-3[f]	18.01	168	98.5	[8]
PM6:Y6	IDIC-C4Ph[g]	18.10	1080	90	[23]
PM6:Y7-BO	Y6-1O[g]	18.11	150	92.5	[24]
PM6:Y6	ITIC-M[h]	18.13	168	97	[25]
PM6:Y6	TIT-2Cl[g]	18.18	2000	79	[26]
PM6:BTP-eC9	BTP-S2[h]	18.31	170	96	[14]
D18-Cl:Y6	G19[i]	18.53	560	90	[12]
PM6:BTP-eC9	MOIT-M[h]	18.5	1500	78	This work

[a]The best PCE of the ternary device. [b]The percentage of PCE after storage vs. initial PCE. [c]The device architecture is ITO/PEDOT:PSS/active layer/PDIN/Al. [d]The device architecture is ITO/PEDOT:PSS/active layer/PDINO/Al. [e]The device architecture is ITO/ZnO/ active layer/MoO_3/Ag. [f]The device architecture is ITO/PEDOT:PSS/active layer/PDINN/Ag. [g]The device architecture is ITO/PEDOT:PSS/active layer/PDIN/Ag. [h]The device architecture is ITO/PEDOT:PSS/active layer/PFN-Br/Ag. [i]The device architecture is ITO/ZnO/ active layer/MoO_3/Al.

Table S6. Summary of contact angles (θ), surface tensions (γ) and Flory-Huggins interaction parameters (χ) for PM6, BTP-eC9 and MOITIM films.

Sample	θ_{water}(°)	θ_{DIM}(°)	γ(mN/m)	$\chi^{D\text{-}A}$ [a]	$\chi^{A_1\text{-}A_2}$ [b]
PM6	105.0	53.0	34.25	/	/
BTP-eC9	91.0	43.2	38.04	0.10κ	/
MOIT-M	84.0	37.0	41.11	0.31κ	0.06κ

[a]The Flory-Huggins interaction parameter between the donor (D) and acceptor (A) is calculated through the equation of: $\chi^{D\text{-}A} = \kappa(\sqrt{\gamma_D}-\sqrt{\gamma_A})^2$.

[b]The Flory-Huggins interaction parameter between the two acceptors (A_1 and A_2) is calculated through the equation of: $\chi^{A_1\text{-}A_2} = \kappa(\sqrt{\gamma_{A1}}-\sqrt{\gamma_{A2}})^2$.

Table S7. Summary of the d-spacing and coherence lengths of the in-plane (100) and out-of-plane (010) peaks for blend films.

Active layer	Location (nm^{-1})		d-spacing (nm)		CCL (nm)	
	IP (100)	OOP (010)	IP (100)	OOP (010)	IP (100)	OOP (010)
PM6:BTP-eC9	3.36	17.27	1.87	0.36	11.78	2.52
PM6:BTP-eC9:MOIT-M	3.38	17.39	1.86	0.36	13.15	2.63
PM6:MOIT-M	3.37	17.35	1.86	0.36	13.46	2.73

References

1. M. Zhang, X. Guo, W. Ma, H. Ade and J. Hou, *Adv. Mater.*, 2015, **27**, 4655-4660.
2. W. Su, Q. Fan, X. Guo, J. Chen, Y. Wang, X. Wang, P. Dai, C. Ye, X. Bao, W. Ma, M. Zhang and Y. Li, *J. Mater. Chem. A.*, 2018, **6**, 7988-7996.
3. L. Xu, W. Tao, H. Liu, J. Ning, M. Huang, B. Zhao, X. Lu and S. Tan, *J. Mater. Chem. A.*, 2021, **9**, 11734-11740.

4. Q. An, J. Wang, X. Ma, J. Gao, Z. Hu, B. Liu, H. Sun, X. Guo, X. Zhang and F. Zhang, *Energy Environ. Sci*., 2020, **13**, 5039-5047.
5. Q. Liu, Y. Wang, J. Fang, H. Liu, L. Zhu, X. Guo, M. Gao, Z. Tang, L. Ye, F. Liu, M. Zhang and Y. Li, *Nano Energy*, 2021, **85**, 105963.
6. Y. Zhang, G. Cai, Y. Li, Z. Zhang, T. Li, X. Zuo, X. Lu and Y. Lin, *Adv. Mater.*, 2021, **33**, 2008134.
7. M. Zhang, L. Zhu, C. Qiu, T. Hao, Y. Jiang, S. Leng, J. Chen, G. Zhou, Z. Zhou, Y. Zou, X. Su, Z. Shi, H. Zhu, Y. Zhang, T. P. Russell, X. Zhu and F. Liu, *Small Sci.*, 2021, **2**, 2100092.
8. F. Liu, L. Zhou, W. Liu, Z. Zhou, Q. Yue, W. Zheng, R. Sun, W. Liu, S. Xu, H. Fan, L. Feng, Y. Yi, W. Zhang and X. Zhu, *Adv. Mater.*, 2021, **33**, 2100830.
9. X. Chen, D. Wang, Z. Wang, Y. Li, H. Zhu, X. Lu, W. Chen, H. Qiu and Q. Zhang, *Chem. Eng. J.*, 2021, **424**, 130397.
10. Y. Li, Y. Cai, Y. Xie, J. Song, H. Wu, Z. Tang, J. Zhang, F. Huang and Y. Sun, *Energy Environ. Sci.*, 2021, **14**, 5009-5016.
11. D. Wang, G. Zhou, Y. Li, K. Yan, L. Zhan, H. Zhu, X. Lu, H. Chen and C. Z. Li, *Adv. Funct. Mater.*, 2021, **32**, 2107827.
12. Z. Chen, W. Song, K. Yu, J. Ge, J. Zhang, L. Xie, R. Peng and Z. Ge, *Joule*, 2021, **5**, 2395-2407.
13. Y. Cai, Y. Li, R. Wang, H. Wu, Z. Chen, J. Zhang, Z. Ma, X. Hao, Y. Zhao, C. Zhang, F. Huang and Y. Sun, *Adv. Mater.*, 2021, **33**, 2101733.
14. Y. Li, Y. Guo, Z. Chen, L. Zhan, C. He, Z. Bi, N. Yao, S. Li, G. Zhou, Y. Yi, Y. Yang, H. Zhu, W. Ma, F. Gao, F. Zhang, L. Zuo and H. Chen, *Energy Environ. Sci.*, 2022, **15**, 855-865.

15. J. Wang, M. Zhang, J. Lin, Z. Zheng, L. Zhu, P. Bi, H. Liang, X. Guo, J. Wu, Y. Wang, L. Yu, J. Li, J. Lv, X. Liu, F. Liu, J. Hou and Y. Li, *Energy Environ. Sci.*, 2022, **15**, 1585-1593.
16. S. Bao, H. Yang, H. Fan, J. Zhang, Z. Wei, C. Cui and Y. Li, *Adv. Mater.*, 2021, **33**, 2105301.
17. Y. Cui, Y. Xu, H. Yao, P. Bi, L. Hong, J. Zhang, Y. Zu, T. Zhang, J. Qin, J. Ren, Z. Chen, C. He, X. Hao, Z. Wei and J. Hou, *Adv. Mater.*, 2021, **33**, 2102420.
18. K. N. Zhang, J. J. Guo, L. J. Zhang, C. C. Qin, H. Yin, X. Y. Gao and X. T. Hao, *Adv. Funct. Mater.*, 2021, **31**, 2100316.
19. T. Yan, W. Song, J. Huang, R. Peng, L. Huang and Z. Ge, *Adv. Mater.*, 2019, **31**, 1902210.
20. X. Liao, Q. Xie, Y. Guo, Q. He, Z. Chen, N. Yu, P. Zhu, Y. Cui, Z. Ma, X. Xu, H. Zhu and Y. Chen, *Energy Environ. Sci.*, 2022, **15**, 384-394.
21. B.-H. Jiang, Y.-J. Peng, Y.-W. Su, J.-F. Chang, C.-C. Chueh, T.-S. Shieh, C.-I. Huang and C.-P. Chen, *Chem. Eng. J.*, 2022, **431**, 133950.
22. X. Ma, J. Wang, J. Gao, Z. Hu, C. Xu, X. Zhang and F. Zhang, *Adv. Energy Mater.*, 2020, 2001404.
23. H. Tan, B. Yuan, Z. Shao, W. Deng, J. Yu, M. Xiao, H. Wu and W. Zhu, *Chem. Eng. J.*, 2022, **445**, 136691.
24. H. R. Bai, Q. An, M. Jiang, H. S. Ryu, J. Yang, X. J. Zhou, H. F. Zhi, C. Yang, X. Li, H. Y. Woo and J. L. Wang, *Adv. Funct. Mater.*, 2022, 2200807.
25. Y. Zeng, D. Li, H. Wu, Z. Chen, S. Leng, T. Hao, S. Xiong, Q. Xue, Z. Ma, H. Zhu and Q. Bao, *Adv. Funct. Mater.*, 2021, **32**, 2110743.
26. J. Chen, J. Cao, L. Liu, L. Xie, H. Zhou, J. Zhang, K. Zhang, M. Xiao and F. Huang, *Adv. Funct. Mater.*, 2022, 2200629.